ADVANCED OPTICAL MATERIALS
www.advopticalmat.de

Photonic Bound States in the Continuum: From Basics to Applications

*Shaimaa I. Azzam and Alexander V. Kildishev**

The introduction of bound states in the continuum (BICs) to photonics has revolutionized the way cavity design and light–matter interactions are thought about in general. BICs can have very high quality factors, even in open structures where access to radiation is permissible. Now, BICs found applications in a large class of areas, including nonlinear enhancement, coherent light generation, sensors, filters, integrated circuits, and many others. In this review, the different types of BICs in photonic systems, as well as their physics and formation mechanisms are briefly overviewed. The rest of the review focuses on the current and emerging applications of photonic BICs and their role in shaping the interaction of light and matter.

1. Introduction

Cavity design in optics and photonics has been a long-standing area of investigation due to its paramount importance in both applied and fundamental research. Conventionally, light is confined using a closed or Hermitian system where access to radiation channels is prohibited leading to high quality (Q) factor resonances. In an open or non-Hermitian system, the light waves are coupled to the radiation continuum leading to resonant modes with finite lifetimes. Bound states in the continuum (BICs) are an exception to this traditional understanding. BICs are peculiar states that remain localized with lifetimes that diverge to infinity even though they reside in the radiation continuum. BICs were first mathematically proposed in 1929 by von Neumann and Wigner who constructed an artificial quantum potential to support a BIC—an electronic state with energy that falls above the continuum threshold.[1] Even though the original proposal by von Neumann and Wigner was never practically realized, other BIC formation mechanisms and systems have been theoretically suggested and experimentally demonstrated.[2–10] Although BICs are a general wave phenomenon that have been observed for various waves such as electromagnetic, acoustic, and water waves, this review will focus only on BICs for electromagnetic waves that are supported by photonic systems.

Dr. S. I. Azzam, Prof. A. V. Kildishev
School of Electrical & Computer Engineering
Birck Nanotechnology Center and Purdue Quantum Science and Engineering Institute
Purdue University
West Lafayette, IN 47907, USA
E-mail: kildishev@purdue.edu

The ORCID identification number(s) for the author(s) of this article can be found under https://doi.org/10.1002/adom.202001469.

DOI: 10.1002/adom.202001469

1.1. Quasi- and Near-BICs

In theory, BICs are dark states with infinite radiative lifetime and generally require at least one dimension of the structure extending to infinity.[6] Similar conditions can also be obtained in localized systems of finite extent when the permittivity approaches zero.[5,11] However, in practice, due to the finite extent of structures, material absorption, and other external perturbations, BICs collapse to a Fano resonance with a limited radiative Q factor. Such resonances are known as quasi-BIC and they have been used to obtain very high Q resonances in numerous photonic systems to date.[6,8,12] Even though practical implementations of BICs are limited to quasi-BIC, in the literature, as well as in this review, quasi-BIC are commonly referred to as BICs. Another type of high-Q resonances called near-BIC is obtained in the vicinity of the BIC through detuning the system from the BIC regime.[9,13,14] Near-BICs can be explained by the Theory of Resonance Reactions by Fonda[13,14] as a bound state can exist in the continuum at an energy where some channels are open even when the open and closed channels are strongly coupled. If the Hamiltonian of the system differs slightly from the one that can produce such a bound state, a sharp resonance appears in all scattering and reaction cross-sections. Near-BIC resonances can be obtained over an interval of values of a specific parameter of the system, unlike BICs that are generally achieved at a single value of the parameter.[9,15] This is of importance for practical systems as it provides stability to fabrication errors and other imperfections.[12] It is also worth mentioning that the total Q factor (Q_t) realizable through BICs is generally limited by the material loss. While the radiative Q-factor (Q_r) at BICs can diverge, the non-radiative Q-factor (Q_{nr}) is limited by material absorption and its inhomogeneous broadening, scattering from the structural disorder, and in-plane lateral leakage. It is therefore, important to have an accurate distinction between Q_r and Q_{nr} and account for non-radiative processes as generally the main contributors to the total Q."

1.2. BIC Types and Formation Mechanisms

Since the time of initial prediction of BICs in photonics, they have been realized in numerous geometrical systems, including gratings, waveguides, metasurfaces, and photonic crystals.[4,7,9,16–24] Such a broad diversity of photonic systems supports different types of BICs that originate from various physical mechanisms. We will briefly highlight the different

types of BICs and their physical origins in this section. A more detailed and comprehensive review of the subject can be found in ref. [6]. The physical mechanisms leading to the formation of a BIC can be broadly categorized into three distinct types. The fist and most straightforward type of BICs is formed due to the symmetry or separability.[25–29] The second type includes interference-based BICs in which the destructive interference of resonances leads to the trapped states.[3,4,30–32] Finally, the last type consists of specifically engineered BICs achieved through inverse construction.[33,34]

A state can decouple from the radiation and turn into a BIC if it exhibits a different symmetry with its surroundings. Such a state, know as symmetry-protected BIC, remains localized as long as the symmetry in the system is preserved. Symmetry-protected BICs have been thoroughly examined in a multitude of systems including metasurfaces—subwavelength-thin optical lattices—as well as other periodic structures, such as classical gratings and photonic crystals.[25–28]

BICs with separability of variables have been proposed in ref. [35]; however, their exploration in photonic systems has been quite limited.[29,36] The basic idea of separable BICs is to present the Hamiltonian of a system as a superposition of two or more independent Hamiltonians. Each of the constituent Hamiltonians acts on a single variable and has an eigenvalue that corresponds to a bound state. The product of the bound states of the constituent Hamiltonians forms a BIC with an eigenvalue that is the sum of the eigenvalues of the individual Hamiltonians.

Interference-based BICs or BICs through parameter tuning are the result of the destructive interference between different channels. Tuning a sufficient number of parameters of the system can lead to a complete elimination of the radiation, and hence, to a BIC formation. The interfering channels could be resonances of different resonators, resonances of the same resonator, or even a single resonance. When a lossless resonant structure is coupled to a single radiation channel, its reflection reaches unity near the resonance frequency. If two of these resonators are arranged such that they form a cavity, at a specific frequency or spacing where the wave accumulates a total phase that causes the destructive interference between the two resonances, a BIC would form. Such BICs are called Fabry–Pérot BIC and they have been demonstrated in several photonic systems.[2,3,31,37] The BIC resulting from the interference of two resonances that belong to the same resonator is known as Friedrich–Wintgen (FW) BIC.

Unlike the Fabry–Pérot BICs where the resonances are far apart, the resonances leading to the FW BIC are at the same location and are coupled through the same radiation channel. The spectral location of the FW BIC is generally near the frequency crossings of the uncoupled resonances. And lastly, single-resonance BICs, where a single resonance can turn into a BIC if enough parameters have been tuned. In this case, the resonance itself is believed to originate from two or more waves, and adjusting the parameters of the system that supports such resonance can lead to suppression of radiation.[4]

The third formation mechanism of BICs is based on specifically engineered BICs through inverse construction. This approach dates back to the original proposal of von Neumann and Wigner to realize BICs through the construction of an artificial potential.[1] Constructing a potential profile that can lead to a set of desired BICs in a given system has been later studied in lattice systems to construct BICs localized at the edge of the lattice.[33,34] Engineering BICs through inverse construction can also be achieved by engineering some other feature of the system required to allow for BICs, for example, through engineering the boundary shape of a structure.[38] Inverse construction may generate non-physical or unrealizable systems, and therefore, the experimental realizations of such systems to date have been limited. Moreover, realizing BICs through reverse engineering has not been extensively studied in photonics and thus far we are not aware of any experimental report of such BICs in photonic systems. However, this method may offer a lot of promise for engineering and optimization of synthetic BICs in photonic systems.

1.3. Multipole Approach to the BIC-Based Meta-Elements

The multipole analysis (MA) is a powerful technique for getting a comprehensive understanding of the BIC physics and synthesis of the viable structures supporting the trapped states. The initial studies on the MA of optical metamaterials were performed by several research groups. Early studies include for example the work of Petschulat et al.,[43] where the effective permittivity and permeability was also derived from the analytical expressions for the dispersion, and the electric displacement and magnetization fields. This analytical approach was compared against direct numerical simulations showcasing the advantages and limitations of the proposed approach.

Subsequent works applied the MA to the theoretical and experimental studies of infinite periodic arrays with the particles of regular shapes (see, e.g., refs. [44,45]). Other directions employed the multipole approach in the analysis of isolated particles to either satisfy the Kerker backscattering condition[46] or to enhance non-linear light–matter interaction.[47–49] Along with the photonics theory, the numerical efforts have been advanced in a line of recent MA-relevant and broader studies.[50–54]

Figure 1 gives some representative examples of the multipole analysis of the BIC meta-elements. Figure 1a depicts a general case of a metasurface with a square unit cell with the meta-atoms under test and associated radiation patterns. Comprehensive schematic representations of the formation mechanisms of symmetry protected (at-Γ) and accidental (off-Γ) BICs are depicted in the top and bottom rows of Figure 1b.[39]

Multipolar expansion of the Γ-point BICs: if a single unit cell consists only of the multipoles that do not radiate along the z-axis, then apparently, there is no total radiation in the z direction (Figure 1b, top row). Analyzing the multipoles, the authors in ref. [39] conclude that in the sub-diffractive array all the modes, which do not have the tesseral harmonics with $m = 1$ form symmetry protected BICs. As a concept example, the authors use a published BIC demonstration of lasing achieved with a bi-periodic array of nanoparticles.[55]

A similar approach is applied to the multipolar expansion of accidental BICs; it is shown that every contributing term of the decomposition shall be purely real, then all vector harmonics cancel each other in the direction of a given wavevector $\vec{k}_1$. Hence, similar to the Kerker effect, all the terms should be either in phase or completely in reverse (Figure 1b, bottom

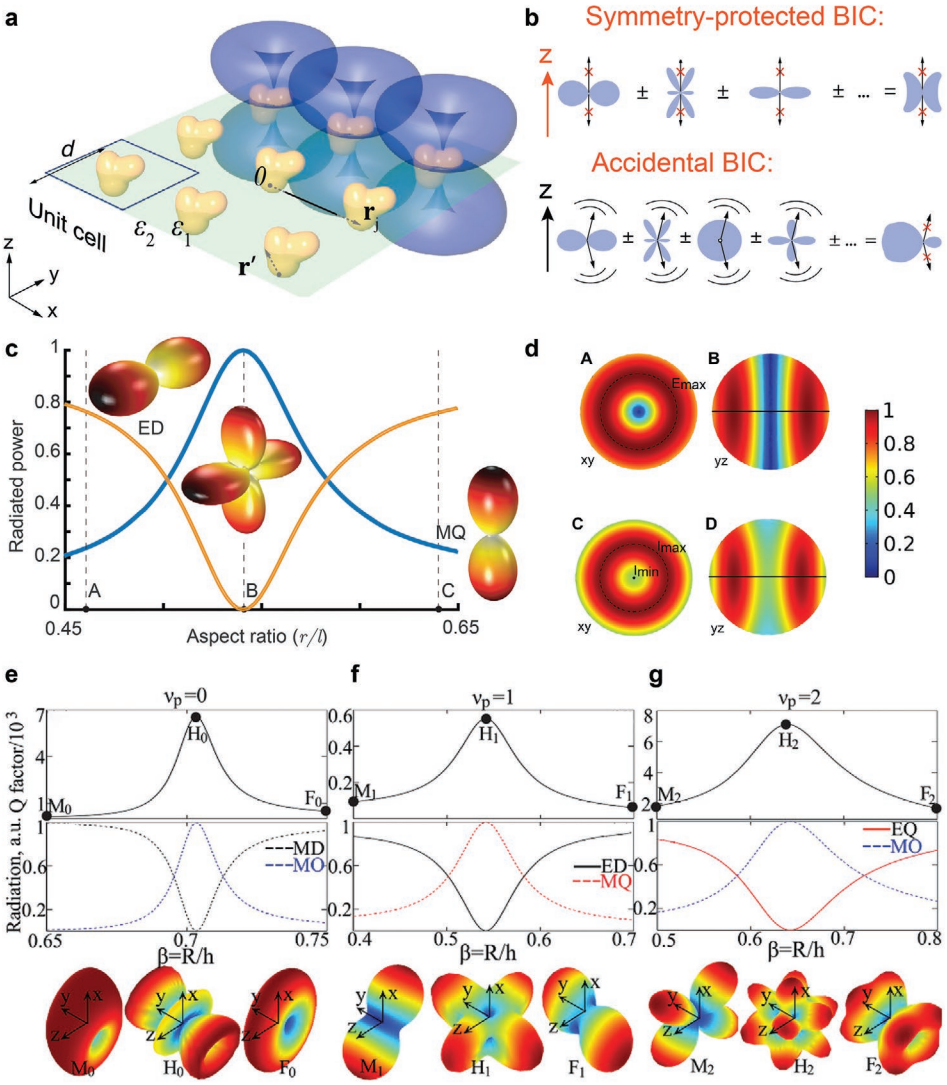

Figure 1. Applying multipole analysis to BIC-based photonic meta-elements. a) A square unit cell with dielectric meta-atoms. b) The formation of symmetry-protected (at-Γ, upper panel) and accidental (off-Γ, lower panel) BICs. (a) and (b) are reproduced with permission.[39] Copyright 2019, American Physical Society. c) The electric dipole (ED) and magnetic quadrupole (MQ) contributions to the radiated power of the $TM_{1,1,1}$ mode in a single-cylinder resonator, and the far-field radiation patterns of $TM_{1,1,1}$ mode at different aspect ratios. (c) is adapted with permission.[40] Copyright 2019, Andrey A. Bogdanov et al., published by SPIE and CLP. d) The spatial distributions of the normalized *E*-field magnitude E/E_{max} (A,B) and the normalized intensity I/I_{max} (C,D) of azimuthally polarized cylindrical vector beam in the focal plane *xy* (A,C) and in the through-focus plane *yz* (B,D). The focal plane in (B,D) is indicated by solid black lines. Dashed black circles delineate maxima of the electric field magnitude E_{max} and intensity I_{max} in the focal plane. I_{min} is the minimal value of the intensity in the focal plane. (d) is adapted with permission.[41] Copyright 2020, Irina Volkovskaya et al., published by De Gruyter, Berlin/Boston. e–g) Evolution of the Q-factors (top row) and the power (middle row) radiated from all non-negligible multipoles for the supermodes of order $v_p \in \{0,1,2\}$ that for *p*-polarized light correspond to the magnetic dipole (MD), electric dipole (ED), and electric quadrupole (EQ).[42] In each column e–g), the supermodes are indicated by points M_{v_p}, H_{v_p}, and F_{v_p}, where $v_p \in \{0,1,2\}$. The corresponding far-field radiation patterns of the supermodes are shown at the bottom row of each column. (e)–(g) are adapted with permission.[42] Copyright 2019, Wiley-VCH.

row). A related toy model, combining the vertical electric dipole and horizontal magnetic dipole that interfere destructively in the direction of $\vec{k}_1$, also provides a comprehensive conceptual understanding of accidental BICs upon *p*-polarized excitation.[8]

We further illustrate the usefulness of the multipole decomposition concept with the parametric optimization of the interplay between the electric dipole (ED) and magnetic quadrupole (MQ) of the $TM_{1,1,1}$ mode in a single-cylinder resonator examined by Bogdanov et al.[40] (Figure 1c). The figure shows contributions to the radiated power, and the far-field radiation patterns of $TM_{1,1,1}$ mode versus different aspect ratios, where the quasi-BIC regime is achieved at point B.[40]

Yet another important application of the multipole analysis approach is the decomposition of the incident radiation depicted in Figure 1d in terms of the vector spherical harmonics.[41] The concept is applied to get the values of the incident multipolar content of the azimuthally polarized cylindrical vector beam, and in particular, its magnetic dipolar and octupolar components. The analysis is then applied to the experimental data published in ref. [56] to optimize the nonlinear interactions.

Finally, the utility of the multipole analysis is illustrated with an extended study of the evolution of the Q-factors in cylindrical resonators (top row) and the power (middle row) radiated from all non-negligible multipoles for their supermodes with the quantum number $\nu_p \in \{0, 1, 2\}$.[42] Figure 1e–g depicts the supermodes indicated by points M_{ν_p}, H_{ν_p}, and F_{ν_p} for $\nu_p \in \{0, \sim 1, \sim 2\}$ with the corresponding far-field radiation patterns shown at the bottom row of each panel. Similar to previous results, the study confirmed that for all ν_p, the Q-factor enhancement is driven by the order conversion from a lower to higher multipole, for example, MD→MO for $\nu_p = 0$ (Figure 1e), ED→MQ, ($\nu_p = 1$, Figure 1f), and EQ→MO ($\nu_p = 2$, Figure 1g). Expanding the results of[39], Chen et al. also demonstrate that i) the position of the maximum Q-factor always coincide with the resonance positions of the dominant the highest-order multipole, ii) away from the maximum, the multipoles are converted from the higher to lower order and decreasing Q-factor, and iii) at the optimum points, the highest achievable Q-factor is defined by the highest order of the dominant multipole (compare for example Q-factors in Figure 1f,g). We may comment that the multipole analysis not only provides the most general means for the comprehensive understanding of BICs, but could also enable new paradigms of data- and physics-driven approaches to optimizing BIC-based high-Q photonic systems.

Following this introduction, we organize the remainder of this paper as follows. Section 2 deals with the applications of BICs in photonics. Subsequently, we analyze and compare the diverse palette of various BIC functionalities that include enhancing optical nonlinearities and lasing, sensing and imaging, beam shaping, and quantum photonics. All this analysis and comparison are done in Sections 2.1–2.4. Section 3 reports on the dynamic control of BICs. As we shall see, the recent progress in the optical and electric control of nonlinear optical materials has greatly affected the subsequent progress in the related BIC research and is now reflected in the relevant authors' contributions. Without being exhaustive on this matter in Section 1, we conclude the paper with a précis covering an outlook of future development in Section 4.

2. Applications of BICs in Photonics

2.1. BICs for Enhancing Optical Nonlinearities

High-Q resonances have been employed to enhance light–matter interaction and boost the efficiency of diverse nonlinear optical phenomena. The flexibility that BICs have introduced to the design and realizations of high-Q resonances in nanophotonic systems has positioned them to benefit the nonlinear photonics community immensely. BICs have thus far been utilized to boost a plethora of nonlinear effects, including the optical Kerr effect,[57,58] lasing action,[18,55,59–64] second- and third-harmonic generation,[56,65–70] four-wave mixing,[65] dynamical nonlinear image tuning,[71] and many more. This section will shed a brief light on the latest advancements pertinent to the role of BICs in intensifying nonlinearities in nanophotonic platforms. We will focus on only two classes of nonlinear interactions; BIC based lasers in Section 2.1.1 and harmonic generation in Section 2.1.2.

2.1.1. BIC-Based Lasers

Applying BICs to the field of lasers has allowed for new opportunities not readily accessible with conventional cavities. The use of the high-Q BIC resonances to provide feedback for lasing has enabled directional, scalable, controllable, and low threshold microlasers.[18,55,59–62] In addition, due to the non-zero topological charges associated with BICs, the laser emission at the BIC points is naturally a vector beam.[63,64] While the first experimental demonstration of BICs in optical structures did not take place until around a decade ago,[4,25,27] BIC-based lasers had been reported long before that. A closer look at many distributed feedback and surface-emitting lasers indicates that they operate at the band edge (i.e., the Γ point, which is a symmetry protected BIC).[72–76] In such lasers, any perturbation that disturbs the symmetry would significantly affect the Q factor of the resonance. Also, as the operation wavelength moves further away from the Γ point, the Q factor of the symmetry protected BIC drops significantly. This is, in general, different from interference-based BICs that are formed with varying a particular continuous parameter of the system, such as the radius of the height of resonators.[1,77]

After the demonstration of BICs in photonics systems, more complex BICs have been exploited to support lasing action. Near-infrared room temperature lasing was demonstrated in a thin membrane of semiconductor material suspended in the air.[18] An InGaAsP multiple quantum wells membrane of cylindrical nanoresonator array suspended in the air was designed to support multiple high-Q modes at the Γ point around the telecommunication wavelength range, **Figure 2**a. The laser was designed to operate around a resonance-trapped BIC at 1551 nm, as depicted in Figure 2b. The BIC-based membrane laser showed low threshold, room temperature, and single-mode operation that are persistent even with varying laser geometrical parameters. More interestingly, the BIC laser still shows great performance even with scaling down the lattice size of the membrane to only 8×8 resonators, suggesting great potential for multicolor on-chip lasing.[18]

Similarly, arrays of dielectric resonators on a substrate have been used to demonstrate lasing based on BIC with controlled directionality.[55] In this array of GaAs resonators, only dipole modes that are orthogonal to the array plane are allowed. These normal-to-lattice dipoles lead to the sub-diffractive regime; the dipoles oscillate only in the normal direction, prohibiting the radiation in this direction, a BIC if formed where no radiation from the system can occur. By increasing the system's periodicity in at least one of the array directions, a leaky channel is opened where diffraction can occur. This enabled control over the directionality of the emitted laser beam. The poor external quantum efficiency of GaAs at room temperature has been avoided in the laser by operating at 77 K. Changing the temperature from 77 to 200 K allowed for tuning the gain spectrum of GaAs, resulting in some tunability of the laser peak in from 830 to 850 nm.

Additionally, BICs have been exploited to demonstrate integrated and steerable-by-design vortex lasers,[63] Figure 2c. In that case, BICs carrying a non-zero topological charge have been controlled by the topology of the lasing structure. In[63] laser light generated at the BIC regime was characterized for its far-field phase singularity, which was used to determine the topological

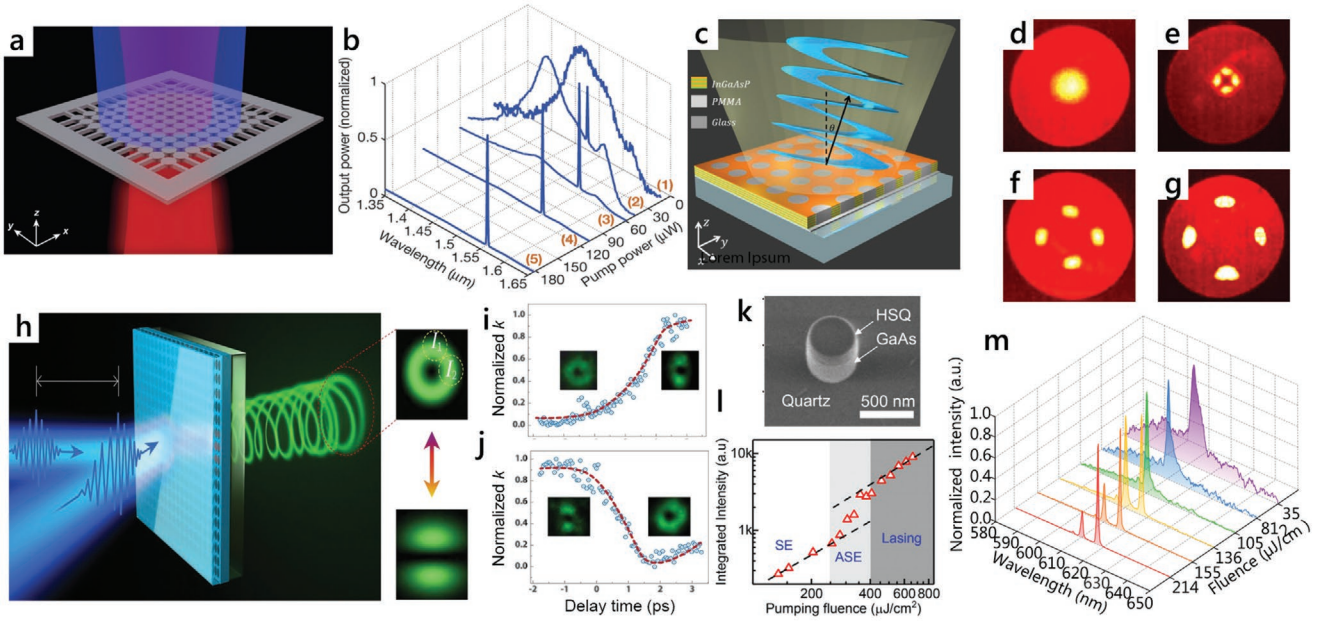

Figure 2. Lasing with BICs. a) Schematic of BIC-based laser membrane illustrating the optical pump beam (blue) and lasing from the BIC mode (red).[18] b) The normalized output laser power as a function of wavelength and pump power from the membrane depicted in (b) showing a single lasing peak at 1,551.4 nm. (a) and (b) are adapted with permission.[18] Copyright 2017, Springer Nature. c) A square lattice photonic crystal structure made of InGaAsP multiple quantum wells bonded on a glass substrate. The structure is optically pumped (yellow beam) and generates a vortex beam at a controllable angle (blue beam).[63] d–g) Measured k-space images of the emission from lasers shown in (c) with different radii. The images show that the emission angle of the lasing increases as the radius of the holes decreases from d) 250 nm, to e) 240 nm, then to f) 225, and finally to g) 190 nm demonstrating beaming of the lasing emission. (c)–(g) are adapted with permission.[63] Copyright 2020, Babak Bahari et al. h) Vortex lasing from a perovskite metasurface.[64] When the array is pumped with one beam, a donut-shaped lasing emission is observed (inset top). When two beams are used for pumping with a temporal delay, the symmetry is broken, and two linearly polarized beams are observed (inset bottom). i) The switching from a vortex laser to linearly polarized laser and j) vice versa. (h)–(j) are reproduced with permission.[64] Copyright 2020, AAAS. k) An SEM image of the single GaAs nanocylinder laser and l) its output emission intensity versus pumping laser fluence showing the transitions from spontaneous emission (SE) to amplified spontaneous emission (ASE) and finally to lasing. (k) and (l) are adapted with permission.[62] Copyright 2020, American Chemical Society. m) Multi-wavelength lasing from arrays of nanoresonators versus the pumping fluence. Adapted with permission.[61] Copyright 2020, Shaimaa I. Azzam et al.

charge of the beams. Self-interference of the lasing beams showed two inverted fork patterns that were translated into a topological charge of +1 and -1 for different types of BICs. Moreover, changing the radius of the holes in such a system led to the continuous movement of the BIC in the reciprocal space showing a steerable-by-design laser light, as can been observed from Figure 2d–g. A similar BIC-based vortex laser made of perovskite that enables ultrafast control was recently demonstrated,[64] Figure 2h. The vortex laser can be switched to linearly-polarized lasing, or vice versa, with switching times as small as one picosecond, as can be observed from Figure 2i,j. Such a laser shows dramatic speed enhancement over directly modulated microlasers allowing for all-optical controllable lasers at high speed.

BIC lasers hold a lot of promise for on-chip integrated, coherent light sources. Future research to achieve efficient tunability and controllability of lasers is very valuable in broadening their scope of applications. Also, miniaturized lasers is another relevant direction for BIC-based cavities.[62] BIC modes can be realized in down-scaled structures by exploiting and engineering their interference, Figure 2k,l. This enables flexibility in the design of lasing cavities that can be on the scale of a few hundred nanometers.[62] Additional exciting advancements in BIC-based lasing include multi-wavelength lasing,[61] Figure 2m, low-threshold room temperature lasers,[60] topological lasers,[59] and many others.

2.1.2. BICs for Harmonic Generation

Harmonic generation is a nonlinear optical process used to create the harmonic frequencies multiple of the fundamental frequency of incoming light.[78–80] In harmonic generation, an intense laser light interacts with a nonlinear material to generate the frequency harmonics. Harmonic generation is instrumental in generating new shorter wavelengths from existing laser sources. However, generally very high laser intensities, strong material nonlinearity, spatial and temporal control over the laser beam are required for efficient harmonic generation. Recent efforts investigating the effects of BICs on harmonic generation have shown that spectral engineering using BICs can result in tremendous enhancement of the nonlinear response.

Recent theoretical proposals have predicted up to several orders of magnitude enhancement in various harmonic generation processes such as second and third harmonic generation,[65–67] as well as four-wave mixing.[65] Third harmonic generation and four-wave mixing from graphene have been shown to dramatically improve upon engineering the pump beam and the generated beam to match BICs simultaneously.[65] Similarly, second harmonic generation from a transition-metal dichalcogenide monolayer coupled to BICs from a grating has been shown to exhibit significant enhancement.[66] In

another study dealing with the conversion efficiency of second-harmonic generation, the nonlinear response from AlGaAs nanostructures has been predicted to experience a significant boost when coupled to BICs.[67] Using mode engineering to tune the fundamental frequency to a BIC resonance, at least a 100-fold improvement of the second-order nonlinear interaction has been achieved. This improvement is in comparison with utilizing the conventional Mie type magnetic dipole resonance. Even more interestingly, combining BIC concepts with specially-engineered substrates have been exploited to boost multifrequency and multistep nonlinear processes.[81] By engineering a multilayer substrate that hosts an epsilon-near-zero (ENZ) material, as shown in **Figure 3**a, the quasi-BIC's high-Q factor can be maximized due to the destructive interference between the out-of-plane magnetic multipole and its image in the substrate. Such structure has shown the ability to increase the efficiency of third-harmonic generation, four-wave mixing as well as fifth harmonic generation from Silicon disk resonators,[81] Figure 3b.

Experimental demonstrations of BIC-enhanced harmonic generation have followed confirming the numerical predictions.[56,68–70] By breaking the structural symmetry of the nanoresonators arranged in lattice structures, high-Q factor resonances can be obtained from the quasi-BICs in such lattices as shown in Figure 3c–f.[68–70] The structure reported in ref. [69] showed more than five orders of magnitude enhancement of the third harmonic generated for arrays of silicon resonators compared to an unpatterned silicon film of similar thickness. Additionally, the same structure has also demonstrated a significant second harmonic generation signal due to the asymmetry

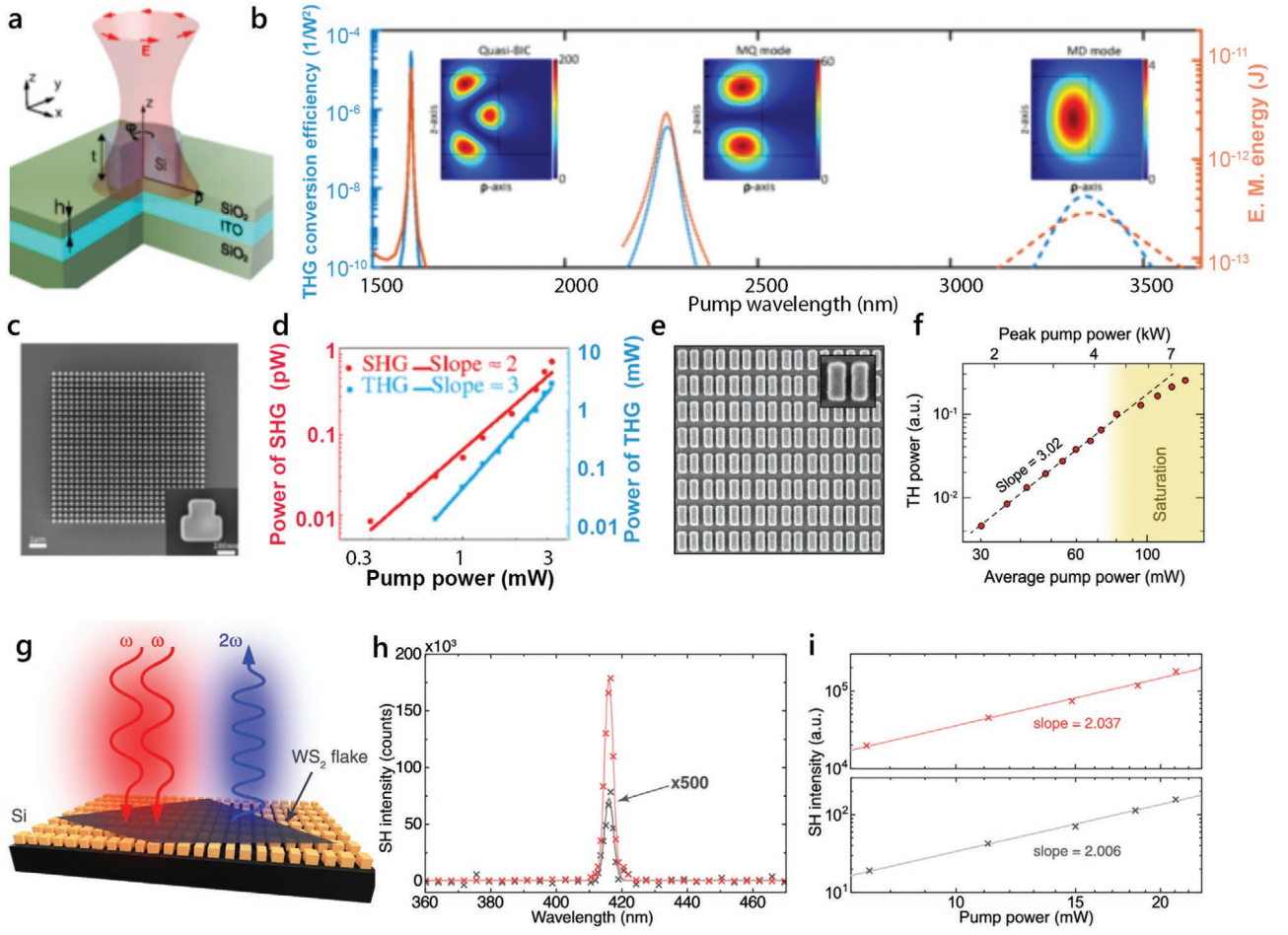

Figure 3. BICs for harmonic generation. a) A schematic of a silicon disk resonator on top of the multilayer substrate hosting a hosts an epsilon-near-zero (ENZ) material.[81] b) The conversion efficiency of third harmonic generation as a function of the pump wavelength close to the quasi BIC, the magnetic quadruple (MQ) mode, and the magnetic dipole(MD) modes. (a) and (b) are adapted with permission.[81] Copyright 2019, Luca Carletti et al., published by the American Physical Society. c) An SEM of the asymmetric silicon metasurface used for second and third harmonic generation in ref. [69]. d) Power dependence of harmonic generation in a logarithmic scale, showing quadratic and cubic power scaling for second and third harmonic, respectively. (c) and (d) are adapted with permission.[69] Copyright 2019, Zhuojun Liu et al., published by the American Physical Society. Similarly, e) the silicon metasurface and f) the cubic scaling of the third harmonic are reported in ref. [68]. (e) and (f) are reproduced with permission.[68] Copyright 2019, American Chemical Society. g) A schematic demonstrating second harmonic generation from a silicon metasurface coupled to a WS_2 monolayer flake.[85] h) The measured second harmonic (SH) intensity spectra from WS_2 monolayers on top of the optimized metasurface (red) compared to that of the reference bulk Si film (gray, magnified 500 ×). i) Measured SH intensities versus the pump power for WS_2 monolayers on top of the metasurface (red) and bulk Si film (gray) (log scale).(g)–(i) are adapted with permission.[85] Copyright 2020, American Chemical Society.

of the resonators and the nonlinearity from the etched silicon surfaces, see Figure 3d. A similar study showed similar findings with a 600-fold enhancement of third-harmonic generation from silicon arrays compared to bare films.[70] The experimental verification of[81] has been carried our recently confirming an enhanced second-harmonic generation from individual AlGaAs nanoscale resonators.[56] Using a combination of quasi-BIC on an ENZ substrate enabled a relatively high-Q factor in the telecommunication regime. Besides, the illuminating light has been engineered to achieve maximum light coupling to the quasi-BIC mode using an azimuthally polarized beam. The study reports two orders of magnitude enhancement for the second harmonic generation compared to other techniques agreeing with the theoretical predictions.[81] Moreover, BICs have also been utilized to enhance not only lower-order harmonics, but also higher optical harmonic generations in photonic devices. As described earlier, through the meticulous engineering of nanophotonic systems that host high-Q resonances at or near the BIC, multifrequency, and multistep nonlinear processes can be enhanced.[81] Recently, this has also been experimentally explored where optical harmonics up to the 11^{th} order have been observed from metasurfaces operating around the BIC.[82] This is an exciting area of application for BICs where the strong light–matter interaction could lead to new techniques for solid-state attosecond spectroscopy and novel extreme UV sources.

In addition, BICs have been used to enhance the nonlinear light–matter interactions in 2D materials. The second-order nonlinear susceptibility of monolayer transition metal dichalcogenides (TMDC) is reported to be more significant compared to bulk nonlinear crystals.[83,84] However, the effective utilization of the high nonlinearity of monolayer TMDC is hindered by their ultra-thin atomic-level thickness. Interfacing TMDC monolayers to judiciously designed nanophotonic devices has been shown to enhance their interaction strength with light and therefore improve their effective nonlinear response.[84] Recently, a dielectric metasurface supporting BICs interfaced with a WS_2 monolayer has been demonstrated to enhance its effective nonlinear susceptibility,[85] Figure 3g. The intensity of the second harmonic generation from the metasurface-monolayer structure has been shown to exhibit more than three orders of magnitude boost compared to the WS_2 monolayer on a flat substrate as demonstrated in Figure 3h,i.

All such advances in nonlinear optics and photonics can have an immense impact on a variety of fields including nonlinear microscopy, all-optical computing and signal processing, and many others. One significant area of applications of BIC-boosted nonlinear light–matter interactions can be quantum photonic technologies, highlighted in Section 2.4.

2.2. BICs for Light Guiding

The quest for the realization of high-efficiency optical waveguides has been fueled by numerous practical motivations, ranging from the need for low-loss optical fibers, the backbone of the internet as we know it, to the demand for photonic integrated chips, the emerging building blocks of new optical computing and information processing paradigms. BICs have the potential to revolutionize the way optical waveguides are designed and how they operate. Generally, light is confined in the high refractive index surrounded by lower refractive index substrate/superstrate.[86] This, however, leads to numerous limitations. For example, many desirable high-index materials, such as diamond or silicon carbide, are very challenging to pattern, and their performance may degrade after fabrication. Also, high-index materials photonics suffers from polarization sensitivity causing the waveguide to respond differently to different light polarizations.[87–91] Polarization sensitivity inhibits the coupling of integrated photonic circuits to fibers as the polarization state changes randomly in optical fibers.[87]

BIC-based photonics elements can guide light through open structures with access to radiation channels. Therefore, light guiding through BICs can relax the conditions imposed on the current waveguides. For example, light can be guided in low-refractive-index materials on high-refractive-index substrates. Since the BIC confinement does not depend on the spatial profile of the structure, the challenges in patterning and fabrication are alleviated, especially for hard to pattern materials such as diamond. It may also relax the precision requirements of the fabrication process. Low-refractive-index light guiding through BICs have been proposed to realize coupling between a low-index polymer and a high-index diamond membrane,[92] **Figure 4**a. Through engineering a continuum of extended waves inside the diamond membrane, and imposing a potential well via the low-index polymer, BICs are formed by controlling the relative phase between the lossy channels to realize destructive interference, as illustrated in Figure 4b.

This is shown in Figure 4c where the coupling strength (g_{20}) and the propagation length (L) of the bound mode are calculated as a function of the polymer strip width (w). It is clear that at specific w values, the BIC is almost completely decoupled from the continuum. The same concept has been applied to microresonators made of the low-refractive-index waveguide on a high-refractive-index substrate. The whispering gallery modes supported by such BIC-based microresonators have been shown to exhibit very high Q factors due to the cancellation of the loss at the BIC points. Key elements for photonic integrated circuits such as waveguides, microcavities, directional couplers, (de)multiplexers, and modulators have recently been experimentally demonstrated in low-refractive-index waveguides on high-refractive-index substrates.[93,98–100] A schematic of the envisioned photonic integrated circuits relying on BIC low-refractive-index waveguides on high-refractive-index substrates is depicted in Figure 4d. This platform used an easy-to-etch organic polymer on top of a lithium niobate layer where the light is guided.[93]

Another type of waveguiding mechanism relying on BICs is the localization of Bloch surface-localized eigenstates in photonic crystals,[4,101,102] Figure 4e–h. BICs in these systems are achieved by the destructive interference between different leakage channels, for example, the forward and back-reflected leakage of a particular mode, leading to a BIC with diverging quality factors. Even though light propagation and waveguiding through photonic crystals is very well established,[103–107] trapping and propagating light above the light-line through BICs offer a unique set of advantages such as a large surface area,

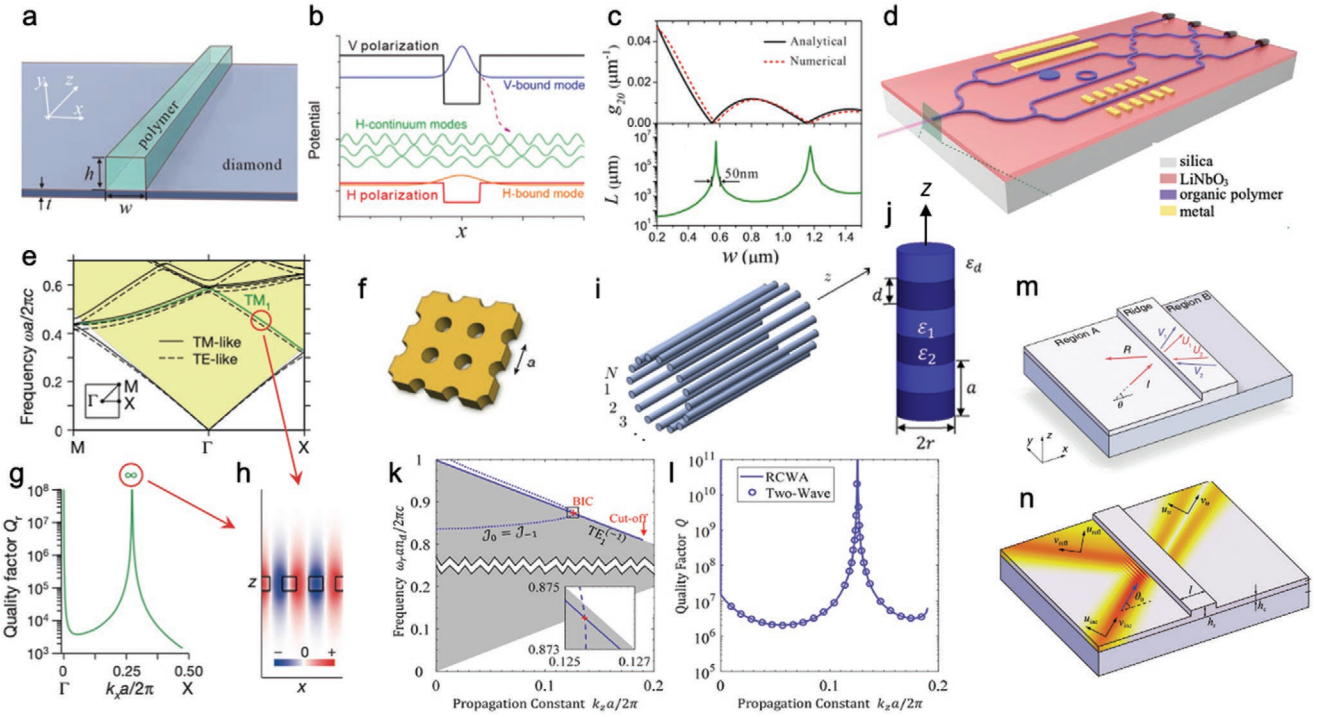

Figure 4. Waveguides and light routing based on BICs. a) A schematic of a low-refractive-index polymer on a high-refractive-index substrate.[92] b) The effective potential of both vertical (V) and horizontal (H) polarized modes. c) The coupling strength g_{20} (top) and the propagation length of the bound waveguide mode (L) (bottom) versus the waveguide width w. (a)–(c) are adapted with permission.[92] Copyright 2014, Wiley-VCH. d) Conceptual illustration of the photonic integrated circuits with BICs based on the low-refractive-index polymer on a high-refractive-index substrate. Adapted with permission.[93] Copyright 2019, Optical Society of America. e) The band structure of the photonic crystal depicted in (f).[4] The BIC is marked with a red circle, and the inset indicates the Brillouin zone. g) Normalized radiative lifetime Q of the TM band shown in (e) as a green line. h) The electric field profile (E_z) of the BIC plotted at $y = 0$. (e)–(h) are adapted with permission.[4] Copyright 2013, Springer Nature. i) A circular array of dielectric cylinders forming an optical fiber. Adapted with permission.[94] Copyright 2018, American Physical Society. j) An optical fiber consisting of a periodic Bragg grating of two dielectrics with relative permittivities ε_1 and ε_2, the core is surrounded by a cladding with relative permittivity ε_d.[95] k) Band structure and l) quality factor of the $TE_1^{(-1)}$ eigenmode of the optical fiber depicted in (j). The quality factor diverges at $k_z = 0.126(2\pi/a)$ where the leaky mode turns into a BIC. (j)–(l) are adapted with permission.[95] Copyright 2019, American Chemical Society. m) The geometry of the integrated Gires–Tournois interferometer. The arrows show the propagation directions of the modes; red arrows show TE-polarized modes and blue arrows show TM-polarized modes. Adapted with permission.[96] Copyright 2020 Evgeni A. Bezus et al., published by De Gruyter, Berlin/Boston. n) A ridge waveguide that can be employed for the spatial integration as well as the differentiation of incident light beams. Adapted with permission.[97] Copyright 2018, Optical Society of America.

and strong electromagnetic confinement near the surface, excitation from free space, along with the selectivity of the wavelength, wavevector, and Q factor.

BICs have also been employed in optical fiber structures with a guiding mechanism alternative to total internal reflection.[94,95] A circular periodic array of silicon dielectric cylinders, depicted in Figure 4i has been numerically simulated to support near-BICs with a propagation mode along the axes of the cylinders.[94] Another optical fiber structure with periodic Bragg gratings with very small index contrasts has been explored in,[95] Figure 4j. A fiber core is an axially-symmetric and 1D-periodic arrangement of two dielectrics with a refractive index contrast of 5×10^{-3} surrounded by a dielectric cladding. The formation of a BIC is a result of the destructive interference of the modes at the core-cladding interface abating the mode that carries outgoing radiation into the cladding, Figure 4k,l.

Moreover, various on-chip photonic functionalities that rely on the rich physics of BICs have also been proposed.[96,97,108–111] Examples include integrated Gires–Tournois interferometer,[96] shown in Figure 4m, spatial integration and differentiation of optical beams,[97] Figure 4n, integrated filters,[109] and many more.

2.3. BICs for Sensing and Imaging

Due to the physical nature of the BIC phenomenon, quasi- and near-BIC states exhibiting high Q-factors in the visible and near-infrared wavelengths are highly sensitive to the change in the dielectric contrast, that is, to the change in their environment. Such a high sensitivity has stimulated an interest in using BICs for biosensing applications[112,113] and refractive index (RI) sensors.[114–116] One of the advantages of BIC-based sensor systems is the potential to be directly excited with external light sources without the need for special coupling mechanisms. This feature puts BIC-based sensors ahead of conventional ones that suffer from coupling loss and a lower volume of light–matter interaction.

Single and double layer silicon photonic crystals was demonstrated as RI sensors with a detection limit as low as 6×10^{-5} refractive index unit in the near-infrared.[114] Utilizing BICs for sensing in photonic crystals versus conventional defect-based photonic crystal sensors exhibited lower radiation loss and stronger light interactions between the light and the analyte. A similar study showed sensing with BIC resonances in both

visible and near-infrared regimes.[115] Direct detection of a monolayer of ultralow-molecular-weight molecules was performed with a large-area photonic crystal sensor tuned to operate at a quasi-BIC regime.

Germanium-based metasurfaces operating at the quasi-BIC were realized for detecting the molecular absorption fingerprints over a broad range of IR wavelengths.[113] The spectral positions of the resonances were controlled with the incidence angle enabling a single metasurface to perform angle-dependent reflectance measurements retrieving the full spectral content of the molecular absorption fingerprint. Another significant advantage of such a BIC-based sensing technique is that it can be implemented using a broadband incoherent light source and a detector to enable the spectrometer-free retrieval of the molecular fingerprints. Finally, the metasurface was shown to provide distinctive absorption signatures of different analytes, including ODAM proteins, DNA aptamers, and polylysine.[113]

Hybrid BICs that form due to the coupling of plasmonic and photonic modes might enable a superior performance to those in all-dielectric systems.[116] In a hybrid waveguide that supports propagating photonic modes and plasmonic modes, an avoided crossing indicating the strong coupling of the photonic and plasmonic modes is observed. A hybrid BIC is formed where the radiation loss is suppressed due to the destructive interference between the plasmonic and a photonic modes. The recent study suggests that hybrid BICs may be superior to those in all-dielectric systems in sensing applications.[116] An order of magnitude enhancement in sensitivity was observed for hybrid BICs compared to purely dielectric BICs. In addition to high-Q factors at the BIC points, hybrid BICs enjoy strong field confinement due to the system's plasmonic component. Moreover, due to the material loss, the quality factor of hybrid BIC is non-divergent, which suggests that hybrid BICs are more suitable for higher integration densities than purely dielectric ones.

2.4. BICs for Quantum Photonics

Nanophotonics provides a very attractive platform for exploring numerous quantum effects and applications.[117–123] Interfacing real or artificial atoms to nanophotonic devices can enable control over the properties of photons, the nature of their transport, and their correlations. It also allows enhancing the photon–photon interactions enabling efficient devices realizations at low power levels. Nanophotonics also provides a scalable, low-power and on-chip means to study fundamental quantum phenomena,[117] generate quantum light,[124,125] realize quantum-optical networks,[121] and much more.

While the exploration of BIC-based devices in quantum photonics is still at a very early stage, the arbitrarily high Q factors realizable at BICs can play a significant role in enhancing light–matter interaction for quantum applications. A proposal to generate entangled photons from monolayer WS_2 via BICs predicted an immense improvement in the generation efficiency compared to conventional parametric down-conversion[126]. By designing a BIC-supporting photonic crystal that allows both signal and idler to correspond to BICs, a theoretical improvement of up to seven orders of magnitude of the generation efficiency of entangled photons has been predicted.[126] Similarly, entangled photon pairs are generated through spontaneous parametric down-conversion from AlGaAs nonlinear metasurfaces operating at the BIC.[127] The enhancement obtained through metasurfaces removes the need for strict phase-matching conditions leading to the possibility of generating entangled photons at high speed.

The enhancement of emission from color centers has been at the heart of single-photon sources.[128,129] BICs were demonstrated to boost the interaction of light with silicon to enhance the photoluminescence from carbon G-center in a silicon metasurface.[130] Matching the G-center peak with the optical resonance from the quasi BIC, a 40-fold enhancement of photoluminescence was experimentally achieved, compared to a non-resonance reference sample. This promising approach to exploit BICs to enhance and manipulate the emission of color centers using the high Q-factor and small mode volumes offered by BIC-supporting nanophotonic devices has been recently discussed in refs. [131,132].

Moreover, strong light–matter interaction has also been explored utilizing BICs through the coupling of excitons in 2D materials to light modes.[133–135] The strong coupling of light and excitons lead to forming exciton-polaritons which are half-light half-matter composite bosons with unique electronic and photonic properties.[136–138] The ability to efficiently realize and control BIC-based polaritons will expand the pool of devices where polaritons can be studied. It will also enable BIC-enhanced light–matter interactions with 2D materials in nonlinear and quantum photonic applications.

2.5. BICs for Beam Shaping

The manipulation of the properties of optical beams such as spatial profile,[139–141] irradiance, phase, velocity,[142] and propagation range[143,144] has been a center of a lot of scientific interest for long time. Beam shaping find applications in light-sheet fluorescence microscopy,[145–147] lithography,[148,149] material processing,[150,151] optical communications,[152–154] optical computing,[155] and many others. The quest for shaping optical beams with compact, integrated devices has led to many innovative ways for manipulating light beams, including, for example, plasmonics[156,157] and metasurfaces.[158,159]

The topological nature of BICs allows to generate optical beams with special properties, such as vortex beams[8,160,161] and diffraction-less beams.[162] BICs are the vortex centers in the polarization direction of the far-field radiation in momentum space that are associated with a conserved and quantized topological number. Such a topological number is defined by a winding number of the polarization vectors around the vortex center.[160,163] The topological origins of BICs stabilize them against perturbations ensuring their robust existence. Besides, the conservation of the topological charges connects the creation, evolution, and annihilation of BICs to their topological properties. This eliminates the need for precise device alignment and makes BIC-generated beams more robust to fabrication imperfections.

In addition to BIC-based vortex lasers discussed in Section 2.1.1, additional studies demonstrating the polarization singularity associated with BICs have been reported.[8,160]

An in-depth understanding of the polarization nature of BICs in the momentum space as well as their topological charges allow engineering photonic devices with desirable and controllable resonance behavior. Another example of the BIC-assisted beamforming technique shows that BICs can aid in the realization of on-chip diffraction-free waveguiding beyond total internal reflection.[162] Through engineering the spatial dispersion of the photonic host to mitigate in-plane diffraction while simultaneously operating at the BIC regime where out-of-plane scattering is prohibited, light can be guided even above the light-line.

3. Tunability and Dynamic Control of BICs

The tunability of optical devices has long been a topic of interest in the photonic community due to the vast scope of applications.[159,164–172] The ability to adjust the functionality of an already fabricated device could allow offsetting fabrication errors and fine-tuning its response. In addition, stable and reversible reconfigurability can enable critical applications such as switching, modulation, computing, sensing, and tunable light sources. Investigations into the tuning mechanisms have spanned electric[173–175], magnetic,[165,176] thermal,[167,177,178] mechanical,[177,179,180] optical ,[166,181,182] or combination[183,184] of these means for controlling the response of optical devices. Combining the high-Q resonances achievable through quasi- and near BICs with the various tuning techniques has recently gained interest due to potential applications.[184–186] While experimental demonstrations of reversible tunability of BIC resonances in the visible is still missing, numerical proposals[184,187] and Terahertz demonstrations have been introduced.[185,186]

Terahertz metasurfaces operating at the quasi-BIC regime have been shown to enable dynamic control of the high-Q resonances upon optical pumping.[185,186] Optical pumping leads to the photoinduced modulation of the Si dielectric function resulting in a continuous modulation of the resonance intensity and Q factor with changing the pump fluence. The optical pumping has been realized with a source photon energy above the silicon's bandgap.[185,186] Due to the increasing nonradiative loss rate upon optical pumping, the Q factor of the resonances with increased pump power was reduced, and the amplitude of the resonance decreased. Such a technique can be broadly utilized to control the response of optical devices in real-time with ultrafast speeds.

Another direction for achieving dynamic control over devices is the incorporation of phase change materials (PCMs). This viable direction can lead to efficient and independent control over the BIC resonances. It has been proposed that the integration of ferroelectric PCMs such as strontium titanate can lead to independent control over the amplitude and frequency of the BIC resonance.[187] In addition, an experimental demonstration of a BIC-based metasurface made of a photosensitive chalcogenide glass has shown tunability of its resonance position.[188] While the change presented in ref. [188] was irreversible, that approach may offer a promising direction for dynamic nanophotonic devices that could enable sensors, modulators, and tunable light sources.

4. Summary and Outlook

With the rise of industrial deployment and societal impact of photonics, an increasing interest is being directed toward the practicality and scalable reproducibility of photonic systems. Low-loss nanoscale metadevices with diverse functionalities have driven the research studies in all-dielectric Fano- and Mie-resonant nanophotonics that has already become a rapidly developing research field. BICs have come along as a promising playground for resonant applications and witnessed such rapid development in both theory and applications of BICs in photonics. This review listed a large number of applications that were investigated as an adaptation of BICs to either improving the system performance or even enabling different physical phenomena. An intricate trapped state available in quasi-BIC resonant photonic nanostructures offers many more novel opportunities for the robust and flexible control of light–matter interaction. A recent example among many others, includes demonstrations of the BIC-based lasing. However, we believe that BIC-related studies remain an active area of research where critical progress has yet to be achieved. BICs still hold immense potential for future applications such as low-energy nonlinearities, quantum photonic interfaces, and active and tunable nanophotonics. We believe that a lot of exciting developments in the optics and photonics are still on the horizon and BICs are well poised to play a role in this future.

Acknowledgements

The authors acknowledge the financial support by the DARPA/DSO Extreme Optics and Imaging (EXTREME) Program under Award HR00111720032. This article is part of the *Advanced Optical Materials* Hall of Fame article series, which recognizes the excellent contributions of leading researchers to the field of optical materials science.

Conflict of Interest

The authors declare no conflict of interest.

Keywords

bound states in the continuum, high Q-factors, light confinement, nonlinear photonics

Received: August 26, 2020
Revised: October 5, 2020
Published online: November 3, 2020

[1] J. von Neumann, E. Wigner, *Phys. Z.* **1929**, *30*, 465.
[2] D. C. Marinica, A. G. Borisov, S. V. Shabanov, *Phys. Rev. Lett.* **2008**, *100*, 183902.
[3] E. N. Bulgakov, A. F. Sadreev, *Phys. Rev. B* **2008**, *78*, 075105.
[4] C. W. Hsu, B. Zhen, J. Lee, S.-L. Chua, S. G. Johnson, J. D. Joannopoulos, M. Soljačić, *Nature* **2013**, *499*, 188.
[5] F. Monticone, A. Alu, *Phys. Rev. Lett.* **2014**, *112*, 213903.
[6] C. W. Hsu, B. Zhen, A. D. Stone, J. D. Joannopoulos, M. Soljačić, *Nat. Rev. Mater.* **2016**, *1*, 16048.

[7] M. V. Rybin, K. L. Koshelev, Z. F. Sadrieva, K. B. Samusev, A. A. Bogdanov, M. F. Limonov, Y. S. Kivshar, *Phys. Rev. Lett.* **2017**, *119*, 243901.
[8] H. M. Doeleman, F. Monticone, W. den Hollander, A. Alù, A. F. Koenderink, *Nat. Photonics* **2018**, *12*, 397.
[9] S. I. Azzam, V. M. Shalaev, A. Boltasseva, A. V. Kildishev, *Phys. Rev. Lett.* **2018**, *121*, 253901.
[10] A. Krasnok, A. Alú, *J. Opt.* **2018**, *20*, 064002.
[11] M. G. Silveirinha, *Phys. Rev. A* **2014**, *89*, 023813.
[12] Z. F. Sadrieva, I. S. Sinev, K. L. Koshelev, A. Samusev, I. V. Iorsh, O. Takayama, R. Malureanu, A. A. Bogdanov, A. V. Lavrinenko, *ACS Photonics* **2017**, *4*, 723.
[13] L. Fonda, *Ann. Phys.* **1961**, *12*, 476.
[14] L. Fonda, *Ann. Phys.* **1963**, *22*, 123.
[15] E. N. Bulgakov, A. F. Sadreev, *Phys. Rev. A* **2018**, *97*, 033834.
[16] S. Weimann, Y. Xu, R. Keil, A. E. Miroshnichenko, A. Tünnermann, S. Nolte, A. A. Sukhorukov, A. Szameit, Y. S. Kivshar, *Phys. Rev. Lett.* **2013**, *111*, 240403.
[17] E. N. Bulgakov, A. F. Sadreev, *Phys. Rev. A* **2014**, *90*, 053801.
[18] A. Kodigala, T. Lepetit, Q. Gu, B. Bahari, Y. Fainman, B. Kanté, *Nature* **2017**, *541*, 196.
[19] L. S. Li, J. Zhang, C. Wang, N. Zheng, H. Yin, *Phys. Rev. A* **2017**, *96*, 013801.
[20] J. Gomis-Bresco, D. Artigas, L. Torner, *Nat. Photonics* **2017**, *11*, 232.
[21] E. Bulgakov, D. Maksimov, P. Semina, S. Skorobogatov, *J. Opt. Soc. Am. B* **2018**, *35*, 1218.
[22] K. Koshelev, S. Lepeshov, M. Liu, A. Bogdanov, Y. Kivshar, *Phys. Rev. Lett.* **2018**, *121*, 193903.
[23] Y. He, G. Guo, T. Feng, Y. Xu, A. E. Miroshnichenko, *Phys. Rev. B* **2018**, *98*, 161112.
[24] Y. Liang, K. Koshelev, F. Zhang, H. Lin, S. Lin, J. Wu, B. Jia, Y. Kivshar, *Nano Lett.* **2020**, *20*, 6351.
[25] F. Dreisow, A. Szameit, M. Heinrich, R. Keil, S. Nolte, A. Tünnermann, S. Longhi, *Opt. Lett.* **2009**, *34*, 2405.
[26] N. Moiseyev, *Phys. Rev. Lett.* **2009**, *102*, 167404.
[27] Y. Plotnik, O. Peleg, F. Dreisow, M. Heinrich, S. Nolte, A. Szameit, M. Segev, *Phys. Rev. Lett.* **2011**, *107*, 183901.
[28] J. Lee, B. Zhen, S.-L. Chua, W. Qiu, J. D. Joannopoulos, M. Soljačić, O. Shapira, *Phys. Rev. Lett.* **2012**, *109*, 067401.
[29] N. Rivera, C. W. Hsu, B. Zhen, H. Buljan, J. D. Joannopoulos, M. Soljačić, *Sci. Rep.* **2016**, *6*, 33394.
[30] Y. Yang, C. Peng, Y. Liang, Z. Li, S. Noda, *Phys. Rev. Lett.* **2014**, *113*, 037401.
[31] V. Liu, M. Povinelli, S. Fan, *Opt. Express* **2009**, *17*, 21897.
[32] X. Gao, C. W. Hsu, B. Zhen, X. Lin, J. D. Joannopoulos, M. Soljačić, H. Chen, *Sci. Rep.* **2016**, *6*, 31908.
[33] M. I. Molina, A. E. Miroshnichenko, Y. S. Kivshar, *Phys. Rev. Lett.* **2012**, *108*, 070401.
[34] N. Gallo, M. Molina, *J. Phys. A: Math. Theor.* **2014**, *48*, 045302.
[35] M. Robnik, *J. Phys. A: Math. Gen.* **1986**, *19*, 3845.
[36] J. Čtyrokỳ, *J. Opt. Soc. Am. A* **2001**, *18*, 435.
[37] R. F. Ndangali, S. V. Shabanov, *J. Math. Phys.* **2010**, *51*, 102901.
[38] M. McIver, *J. Fluid Mech.* **1996**, *315*, 257.
[39] Z. Sadrieva, K. Frizyuk, M. Petrov, Y. Kivshar, A. Bogdanov, *Phys. Rev. B* **2019**, *100*, 115303.
[40] A. A. Bogdanov, K. L. Koshelev, P. V. Kapitanova, M. V. Rybin, S. A. Gladyshev, Z. F. Sadrieva, K. B. Samusev, Y. S. Kivshar, M. F. Limonov, *Adv. Photonics* **2019**, *1*, 016001.
[41] I. Volkovskaya, L. Xu, L. Huang, A. I. Smirnov, A. E. Miroshnichenko, D. Smirnova, *Nanophotonics* **2020**, *9*, 3953.
[42] W. Chen, Y. Chen, W. Liu, *Laser Photonics Rev.* **2019**, *13*, 1900067.
[43] J. Petschulat, C. Menzel, A. Chipouline, C. Rockstuhl, A. Tünnermann, F. Lederer, T. Pertsch, *Phys. Rev. A* **2008**, *78*, 043811.
[44] A. B. Evlyukhin, C. Reinhardt, A. Seidel, B. S. Luk'yanchuk, B. N. Chichkov, *Phys. Rev. B* **2010**, *82*, 045404.
[45] U. Zywietz, A. B. Evlyukhin, C. Reinhardt, B. N. Chichkov, *Nat. Commun.* **2014**, *5*, 3402.
[46] E. Poutrina, A. Urbas, *J. Opt.* **2014**, *16*, 114005.
[47] S. Kujala, B. K. Canfield, M. Kauranen, Y. Svirko, J. Turunen, *Opt. Express* **2008**, *16*, 17196.
[48] A. Capretti, G. F. Walsh, S. Minissale, J. Trevino, C. Forestiere, G. Miano, L. D. Negro, *Opt. Express* **2012**, *20*, 15797.
[49] E. Poutrina, A. Urbas, *Sci. Rep.* **2016**, *6*, 25113.
[50] C. Vrejoiu, *J. Phys. A: Math. Gen.* **2002**, *35*, 9911.
[51] C. Vrejoiu, R. Zus, *J. Phys. A: Math. Theor.* **2010**, *43*, 405208.
[52] P. Grahn, A. Shevchenko, M. Kaivola, *New J. Phys.* **2012**, *14*, 093033.
[53] R. Alaee, C. Rockstuhl, I. Fernandez-Corbaton, *Adv. Opt. Mater.* **2019**, *7*, 1800783.
[54] T. Liu, R. Xu, P. Yu, Z. Wang, J. Takahara, *Nanophotonics* **2020**, *9*, 1115.
[55] S. T. Ha, Y. H. Fu, N. K. Emani, Z. Pan, R. M. Bakker, R. Paniagua-Domínguez, A. I. Kuznetsov, *Nat. Nanotechnol.* **2018**, *13*, 1042.
[56] K. Koshelev, S. Kruk, E. Melik-Gaykazyan, J.-H. Choi, A. Bogdanov, H.-G. Park, Y. Kivshar, *Science* **2020**, *367*, 288.
[57] V. A. Zakharov, A. N. Poddubny, *Phys. Rev. A* **2020**, *101*, 043848.
[58] S. Krasikov, A. Bogdanov, I. Iorsh, *Phys. Rev. B* **2018**, *97*, 224309.
[59] B. Bahari, L.-Y. Hsu, S. Pan, D. Preece, A. Ndao, A. E. Amili, Y. Fainman, B. Kanté, arXiv preprint, arXiv:1904.11873, **2019**.
[60] M. Wu, S. T. Ha, S. Shendre, E. G. Durmusoglu, W.-K. Koh, D. R. Abujetas, J. A. Sánchez-Gil, R. Paniagua-Dominguez, H. V. Demir, A. I. Kuznetsov, *Nano Lett.* **2020**, *20*, 6005.
[61] S. I. Azzam, K. Chaudhuri, A. Lagutchev, Z. Jacob, Y. L. Kim, V. M. Shalaev, A. Boltasseva, A. V. Kildishev, arXiv preprint, arXiv:2006.16473, **2020**.
[62] V. Mylnikov, S. T. Ha, Z. Pan, V. Valuckas, R. Paniagua-Dominguez, H. V. Demir, A. I. Kuznetsov, *ACS Nano* **2020**, *14*, 7338.
[63] B. Bahari, F. Vallini, T. Lepetit, R. Tellez-Limon, J. Park, A. Kodigala, Y. Fainman, B. Kante, arXiv preprint, arXiv:1707.00181, **2017**.
[64] C. Huang, C. Zhang, S. Xiao, Y. Wang, Y. Fan, Y. Liu, N. Zhang, G. Qu, H. Ji, J. Han, L. Ge, Y. Kivshar, Q. Song, *Science* **2020**, *367*, 1018.
[65] T. Wang, X. Zhang, *Photonics Res.* **2017**, *5*, 629.
[66] T. Wang, S. Zhang, *Opt. Express* **2018**, *26*, 322.
[67] L. Carletti, K. Koshelev, C. De Angelis, Y. Kivshar, *Phys. Rev. Lett.* **2018**, *121*, 033903.
[68] K. Koshelev, Y. Tang, K. Li, D.-Y. Choi, G. Li, Y. Kivshar, *ACS Photonics* **2019**, *6*, 1639.
[69] Z. Liu, Y. Xu, Y. Lin, J. Xiang, T. Feng, Q. Cao, J. Li, S. Lan, J. Liu, *Phys. Rev. Lett.* **2019**, *123*, 253901.
[70] C. Zhou, S. Li, C. Gong, Y. Wang, X. Liu, M. Zhan, arXiv preprint, arXiv:2004.01088, **2020**.
[71] L. Xu, K. Zangeneh Kamali, L. Huang, M. Rahmani, A. Smirnov, R. Camacho-Morales, Y. Ma, G. Zhang, M. Woolley, D. Neshev, A. E. Miroshnichenko, *Adv. Sci.* **2019**, *6*, 1802119.
[72] M. Meier, A. Mekis, A. Dodabalapur, A. Timko, R. Slusher, J. Joannopoulos, O. Nalamasu, *Appl. Phys. Lett.* **1999**, *74*, 7.
[73] M. Imada, S. Noda, A. Chutinan, T. Tokuda, M. Murata, G. Sasaki, *Appl. Phys. Lett.* **1999**, *75*, 316.
[74] S. Noda, M. Yokoyama, M. Imada, A. Chutinan, M. Mochizuki, *Science* **2001**, *293*, 1123.
[75] E. Miyai, K. Sakai, T. Okano, W. Kunishi, D. Ohnishi, S. Noda, *Nature* **2006**, *441*, 946.
[76] K. Hirose, Y. Liang, Y. Kurosaka, A. Watanabe, T. Sugiyama, S. Noda, *Nat. Photonics* **2014**, *8*, 406.
[77] H. Friedrich, D. Wintgen, *Phys. Rev. A* **1985**, *32*, 3231.
[78] R. C. Miller, *Appl. Phys. Lett.* **1964**, *5*, 17.
[79] K. Singer, J. Sohn, S. Lalama, *Appl. Phys. Lett.* **1986**, *49*, 248.
[80] S. Ghimire, A. D. DiChiara, E. Sistrunk, P. Agostini, L. F. DiMauro, D. A. Reis, *Nat. Phys.* **2011**, *7*, 138.
[81] L. Carletti, S. S. Kruk, A. A. Bogdanov, C. De Angelis, Y. Kivshar, *Phys. Rev. Res.* **2019**, *1*, 023016.

[82] G. Zograf, K. Koshelev, A. Zalogina, V. Korolev, D.-Y. Choi, M. Zurch, C. Spielmann, B. Luther-Davies, D. Kartashov, S. Makarov, S. Kruk, Y. Kivshar, arXiv preprint, arXiv:2008.11481, **2020**.
[83] M. Weismann, N. C. Panoiu, *Phys. Rev. B* **2016**, *94*, 035435.
[84] H. Chen, V. Corboliou, A. S. Solntsev, D.-Y. Choi, M. A. Vincenti, D. De Ceglia, C. De Angelis, Y. Lu, D. N. Neshev, *Light: Sci. Appl.* **2017**, *6*, e17060.
[85] N. Bernhardt, K. Koshelev, S. White, K. W. C. Meng, J. E. Fröch, S. Kim, T. T. Tran, D.-Y. Choi, Y. Kivshar, A. Solntsev, *Nano Lett.* **2020**, *20*, 5309.
[86] K. Okamoto, *Fundamentals of Optical Waveguides*, Academic Press, Burlington, MA **2006**.
[87] T. Barwicz, M. R. Watts, M. A. Popović, P. T. Rakich, L. Socci, F. X. Kärtner, E. P. Ippen, H. I. Smith, *Nat. Photonics* **2007**, *1*, 57.
[88] S. I. Azzam, S. S. Obayya, *Opt. Lett.* **2015**, *40*, 1061.
[89] S. I. Azzam, M. F. O. Hameed, N. F. Areed, M. M. Abd-Elrazzak, H. El-Mikaty, S. S. Obayya, *IEEE Photonics Technol. Lett.* **2014**, *26*, 1633.
[90] S. I. Azzam, S. Obayya, *IEEE Photonics Technol. Lett.* **2015**, *28*, 367.
[91] D. Dai, J. Bauters, J. E. Bowers, *Light: Sci. Appl.* **2012**, *1*, e1.
[92] C.-L. Zou, J.-M. Cui, F.-W. Sun, X. Xiong, X.-B. Zou, Z.-F. Han, G.-C. Guo, *Laser Photonics Rev.* **2015**, *9*, 114.
[93] Z. Yu, X. Xi, J. Ma, H. K. Tsang, C.-L. Zou, X. Sun, *Optica* **2019**, *6*, 1342.
[94] E. Bulgakov, A. Sadreev, *Phys. Rev. B* **2018**, *98*, 085301.
[95] X. Gao, B. Zhen, M. Soljacic, H. Chen, C. W. Hsu, *ACS Photonics* **2019**, *6*, 2996.
[96] D. A. Bykov, E. A. Bezus, L. L. Doskolovich, *Nanophotonics* **2020**, *9*, 83.
[97] E. A. Bezus, L. L. Doskolovich, D. A. Bykov, V. A. Soifer, *Opt. Express* **2018**, *26*, 25156.
[98] Z. Yu, Y. Wang, B. Sun, Y. Tong, J.-B. Xu, H. K. Tsang, X. Sun, *Adv. Opt. Mater.* **2019**, *7*, 1901306.
[99] Z. Yu, Y. Tong, H. K. Tsang, X. Sun, *Nat. Commun.* **2020**, *11*, 2602.
[100] Z. Yu, X. Sun, *Light: Sci. Appl.* **2020**, *9*, 1.
[101] C. W. Hsu, B. Zhen, S.-L. Chua, S. G. Johnson, J. D. Joannopoulos, M. Soljačić, *Light: Sci. Appl.* **2013**, *2*, e84.
[102] Z. Hu, Y. Y. Lu, *J. Opt. Soc. Am. B* **2017**, *34*, 1878.
[103] S. A. Rinne, F. García-Santamaría, P. V. Braun, *Nat. Photonics* **2008**, *2*, 52.
[104] S. G. Johnson, P. R. Villeneuve, S. Fan, J. D. Joannopoulos, *Phys. Rev. B* **2000**, *62*, 8212.
[105] S. Fan, S. G. Johnson, J. Joannopoulos, C. Manolatou, H. Haus, *J. Opt. Soc. Am. B* **2001**, *18*, 162.
[106] F. Haldane, S. Raghu, *Phys. Rev. Lett.* **2008**, *100*, 013904.
[107] B. Temelkuran, E. Ozbay, *Appl. Phys. Lett.* **1999**, *74*, 486.
[108] E. A. Bezus, D. A. Bykov, L. L. Doskolovich, *Photonics Res.* **2018**, *6*, 1084.
[109] L. L. Doskolovich, E. A. Bezus, D. A. Bykov, *Photonics Res.* **2019**, *7*, 1314.
[110] T. G. Nguyen, G. Ren, S. Schoenhardt, M. Knoerzer, A. Boes, A. Mitchell, *Laser Photonics Rev.* **2019**, *13*, 1900035.
[111] H. Xu, Y. Shi, *Laser Photonics Rev.* **2020**, *14*, 1900430.
[112] F. Yesilkoy, E. R. Arvelo, Y. Jahani, M. Liu, A. Tittl, V. Cevher, Y. Kivshar, H. Altug, *Nat. Photonics* **2019**, *13*, 390.
[113] A. Leitis, A. Tittl, M. Liu, B. H. Lee, M. B. Gu, Y. S. Kivshar, H. Altug, *Sci. Adv.* **2019**, *5*, eaaw2871.
[114] Y. Liu, W. Zhou, Y. Sun, *Sensors* **2017**, *17*, 1861.
[115] S. Romano, G. Zito, S. Torino, G. Calafiore, E. Penzo, G. Coppola, S. Cabrini, I. Rendina, V. Mocella, *Photonics Res.* **2018**, *6*, 726.
[116] M. Meudt, C. Bogiadzi, K. Wrobel, P. Görrn, *Adv. Opt. Mater.* **2020**, *8*, 2000898.
[117] S. Spillane, T. Kippenberg, K. Vahala, K. Goh, E. Wilcut, H. Kimble, *Phys. Rev. A* **2005**, *71*, 013817.
[118] D. Englund, A. Faraon, I. Fushman, N. Stoltz, P. Petroff, J. Vučković, *Nature* **2007**, *450*, 857.
[119] A. D. Greentree, B. A. Fairchild, F. M. Hossain, S. Prawer, *Mater. Today* **2008**, *11*, 22.
[120] J. L. O'brien, A. Furusawa, J. Vučković, *Nat. Photonics* **2009**, *3*, 687.
[121] A. Sipahigil, R. E. Evans, D. D. Sukachev, M. J. Burek, J. Borregaard, M. K. Bhaskar, C. T. Nguyen, J. L. Pacheco, H. A. Atikian, C. Meuwly, R. M. Camacho, F. Jelezko, E. Bielejec, H. Park, M. Loncar, M. D. Lukin, *Science* **2016**, *354*, 847.
[122] M. Atatüre, D. Englund, N. Vamivakas, S.-Y. Lee, J. Wrachtrup, *Nat. Rev. Mater.* **2018**, *3*, 38.
[123] J. Wang, F. Sciarrino, A. Laing, M. G. Thompson, *Nat. Photonics* **2019**, *14*, 273.
[124] T. M. Babinec, B. J. Hausmann, M. Khan, Y. Zhang, J. R. Maze, P. R. Hemmer, M. Lončar, *Nat. Nanotechnol.* **2010**, *5*, 195.
[125] Z. Yuan, B. E. Kardynal, R. M. Stevenson, A. J. Shields, C. J. Lobo, K. Cooper, N. S. Beattie, D. A. Ritchie, M. Pepper, *Science* **2002**, *295*, 102.
[126] T. Wang, Z. Li, X. Zhang, *Photonics Res.* **2019**, *7*, 341.
[127] M. Parry, Y. Xing, L. Xu, A. Poddubny, D. N. Neshev, A. A. Sukhorukov, in *SPIE Micro+ Nano Materials, Devices, and Applications 2019*, Proc. SPIE Vol. 11201, International Society for Optics and Photonics, Washington DC **2019**, p. 112010G.
[128] C. Santori, D. Fattal, J. Vučković, G. S. Solomon, Y. Yamamoto, *Nature* **2002**, *419*, 594.
[129] I. A. Khramtsov, A. A. Vyshnevyy, D. Y. Fedyanin, *npj Quantum Inf.* **2018**, *4*, 15.
[130] L. Zhu, S. Yuan, C. Zeng, J. Xia, *Adv. Opt. Mater.* **2020**, *8*, 1901830.
[131] S. Kolodny, I. Iorsh, *Opt. Lett.* **2020**, *45*, 181.
[132] L. Huang, L. Xu, M. Woolley, A. E. Miroshnichenko, *Adv. Quantum Technol.* **2020**, *3*, 1900126.
[133] K. Koshelev, S. Sychev, Z. F. Sadrieva, A. A. Bogdanov, I. Iorsh, *Phys. Rev. B* **2018**, *98*, 161113.
[134] S. Cao, H. Dong, J. He, E. Forsberg, Y. Jin, S. He, *J. Phys. Chem. Lett.* **2020**, *11*, 4631.
[135] V. Kravtsov, E. Khestanova, F. A. Benimetskiy, T. Ivanova, A. K. Samusev, I. S. Sinev, D. Pidgayko, A. M. Mozharov, I. S. Mukhin, M. S. Lozhkin, Y. V. Kapitonov, A. S. Brichkin, V. D. Kulakovskii, I. A. Shelykh, A. I. Tartakovskii, P. M. Walker, M. S. Skolnick, D. N. Krizhanovskii, I. V. Iorsh, *Light: Sci. Appl.* **2020**, *9*, 56.
[136] H. Deng, G. Weihs, C. Santori, J. Bloch, Y. Yamamoto, *Science* **2002**, *298*, 199.
[137] J. Kasprzak, M. Richard, S. Kundermann, A. Baas, P. Jeambrun, J. Keeling, F. Marchetti, M. Szymańska, R. André, J. Staehli, V. Savona, P. B. Littlewood, B. Deveaud, L. Si Dang, *Nature* **2006**, *443*, 409.
[138] X. Liu, T. Galfsky, Z. Sun, F. Xia, E.-c. Lin, Y.-H. Lee, S. Kéna-Cohen, V. M. Menon, *Nat. Photonics* **2015**, *9*, 30.
[139] J. Durnin, J. Miceli Jr., J. Eberly, *Phys. Rev. Lett.* **1987**, *58*, 1499.
[140] G. Siviloglou, J. Broky, A. Dogariu, D. Christodoulides, *Phys. Rev. Lett.* **2007**, *99*, 213901.
[141] H. E. Kondakci, A. F. Abouraddy, *Phys. Rev. Lett.* **2018**, *120*, 163901.
[142] H. E. Kondakci, A. F. Abouraddy, *Nat. Commun.* **2019**, *10*, 1.
[143] P. T. Rakich, M. S. Dahlem, S. Tandon, M. Ibanescu, M. Soljačić, G. S. Petrich, J. D. Joannopoulos, L. A. Kolodziejski, E. P. Ippen, *Nat. Mater.* **2006**, *5*, 93.
[144] H. E. Kondakci, A. F. Abouraddy, *Nat. Photonics* **2017**, *11*, 733.
[145] F. O. Fahrbach, A. Rohrbach, *Opt. Express* **2010**, *18*, 24229.
[146] F. O. Fahrbach, A. Rohrbach, *Nat. Commun.* **2012**, *3*, 632.
[147] T. Vettenburg, H. I. Dalgarno, J. Nylk, C. Coll-Lladó, D. E. Ferrier, T. Čižmár, F. J. Gunn-Moore, K. Dholakia, *Nat. Methods* **2014**, *11*, 541.
[148] H. Pfeiffer, *J. Vac. Sci. Technol.* **1978**, *15*, 887.
[149] K. Jain, in *Laser Beam Shaping III*, Proc. SPIE Vol. 4770, International Society for Optics and Photonics, Washington DC **2002**, pp. 1–12.

[150] Z. Kuang, J. Li, S. Edwardson, W. Perrie, D. Liu, G. Dearden, *Opt. Lasers Eng.* **2015**, *70*, 1.
[151] D. Liu, Y. Wang, Z. Zhai, Z. Fang, Q. Tao, W. Perrie, S. P. Edwarson, G. Dearden, *Opt. Laser Technol.* **2018**, *102*, 68.
[152] G. A. Koepf, in *Optical Technology for Microwave Applications I*, Proc. SPIE Vol. 477, International Society for Optics and Photonics, Washington DC **1987**, pp. 75–81.
[153] J. Sun, E. Timurdogan, A. Yaacobi, E. S. Hosseini, M. R. Watts, *Nature* **2013**, *493*, 195.
[154] M. J. Heck, *Nanophotonics* **2017**, *6*, 93.
[155] J. Jahns, S. H. Lee, *Optical Computing Hardware: Optical Computing*, Academic Press, San Diego, CA **2014**.
[156] N. Yu, R. Blanchard, J. Fan, Q. J. Wang, C. Pflügl, L. Diehl, T. Edamura, S. Furuta, M. Yamanishi, H. Kan, F. Capasso, *IEEE Trans. Nanotechnol.* **2009**, *9*, 11.
[157] S. Keren-Zur, O. Avayu, L. Michaeli, T. Ellenbogen, *Acs Photonics* **2016**, *3*, 117.
[158] B. Desiatov, N. Mazurski, Y. Fainman, U. Levy, *Opt. Express* **2015**, *23*, 22611.
[159] A. M. Shaltout, V. M. Shalaev, M. L. Brongersma, *Science* **2019**, *364*, 6441.
[160] E. N. Bulgakov, D. N. Maksimov, *Phys. Rev. A* **2017**, *96*, 063833.
[161] B. Wang, W. Liu, M. Zhao, J. Wang, Y. Zhang, A. Chen, F. Guan, X. Liu, L. Shi, J. Zi, *Nat. Photonics* **2020**, *14*, 623.
[162] Y. Lin, T. Feng, S. Lan, J. Liu, Y. Xu, *Phys. Rev. Appl.* **2020**, *13*, 064032.
[163] B. Zhen, C. W. Hsu, L. Lu, A. D. Stone, M. Soljačić, *Phys. Rev. Lett.* **2014**, *113*, 257401.
[164] Y. Zhao, Y. Ying, Q. Wang, *Opt. Laser Technol.* **2014**, *64*, 278.
[165] J. Ge, L. He, J. Goebl, Y. Yin, *J. Am. Chem. Soc.* **2009**, *131*, 3484.
[166] M. Artoni, G. La Rocca, *Phys. Rev. Lett.* **2006**, *96*, 073905.
[167] K. Yoshino, Y. Shimoda, Y. Kawagishi, K. Nakayama, M. Ozaki, *Appl. Phys. Lett.* **1999**, *75*, 932.
[168] Z. Li, Y. Zhou, H. Qi, Q. Pan, Z. Zhang, N. N. Shi, M. Lu, A. Stein, C. Y. Li, S. Ramanathan, N. Yu, *Adv. Mater.* **2016**, *28*, 9117.
[169] S. Abdollahramezani, O. Hemmatyar, H. Taghinejad, A. Krasnok, Y. Kiarashinejad, M. Zandehshahvar, A. Alù, A. Adibi, *Nanophotonics* **2020**, *9*, 1189.
[170] M. Taghinejad, W. Cai, *ACS Photonics* **2019**, *6*, 1082.
[171] T. Cui, B. Bai, H.-B. Sun, *Adv. Funct. Mater.* **2019**, *29*, 1806692.
[172] R. Paniagua-Domínguez, S. T. Ha, A. I. Kuznetsov, *Proc. IEEE* **2019**, *108*, 749.
[173] A. Figotin, Y. A. Godin, I. Vitebsky, *Phys. Rev. B* **1998**, *57*, 2841.
[174] M. W. Haakestad, T. T. Alkeskjold, M. D. Nielsen, L. Scolari, J. Riishede, H. Engan, A. Bjarklev, *IEEE Photonics Technol. Lett.* **2005**, *17*, 819.
[175] E. Penzo, S. Romano, Y. Wang, S. Dhuey, L. Dal Negro, V. Mocella, S. Cabrini, *J. Vac. Sci. Technol. B* **2017**, *35*, 06G401.
[176] C. Xu, X. Hu, Y. Li, X. Liu, R. Fu, J. Zi, *Phys. Rev. B* **2003**, *68*, 193201.
[177] X. Li, A. Das, D. Bi, *Proc. Natl. Acad. Sci. USA* **2018**, *115*, 6650.
[178] K. Chaudhuri, U. Guler, S. I. Azzam, H. Reddy, S. Saha, E. E. Marinero, A. V. Kildishev, V. M. Shalaev, A. Boltasseva, *ACS Photonics* **2020**, *7*, 472.
[179] A. Yang, A. J. Hryn, M. R. Bourgeois, W.-K. Lee, J. Hu, G. C. Schatz, T. W. Odom, *Proc. Natl. Acad. Sci. USA* **2016**, *113*, 14201.
[180] S. Kim, V. Gopalan, *Appl. Phys. Lett.* **2001**, *78*, 3015.
[181] D. Sridharan, R. Bose, H. Kim, G. S. Solomon, E. Waks, *Opt. Express* **2011**, *19*, 5551.
[182] X. Hu, Q. Zhang, Y. Liu, B. Cheng, D. Zhang, *Appl. Phys. Lett.* **2003**, *83*, 2518.
[183] M. C. Huang, Y. Zhou, C. J. Chang-Hasnain, *Nat. Photonics* **2008**, *2*, 180.
[184] M. M. Salary, H. Mosallaei, *ACS Photonics* **2020**, *7*, 1813.
[185] K. Fan, I. V. Shadrivov, W. J. Padilla, *Optica* **2019**, *6*, 169.
[186] S. Han, L. Cong, Y. K. Srivastava, B. Qiang, M. V. Rybin, A. Kumar, R. Jain, W. X. Lim, V. G. Achanta, S. S. Prabhu, Q. J. Wang, Y. S. Kivshar, R. Singh, *Adv. Mater.* **2019**, *31*, 1901921.
[187] X. Chen, W. Fan, *Nanomaterials* **2020**, *10*, 623.
[188] E. Mikheeva, K. Koshelev, D.-Y. Choi, S. Kruk, J. Lumeau, R. Abdeddaim, I. Voznyuk, S. Enoch, Y. Kivshar, *Opt. Express* **2019**, *27*, 33847.

Shaimaa Azzam is a postdoctoral fellow at the California NanoSystems Institute in the University of California Santa Barbara. She received her Ph.D. degree from the Department of Electrical and Computer Engineering, Purdue University in 2020. Her research interests are in nanophotonics, where she studies fundamentals and applications of light–matter interactions at the nanoscale.

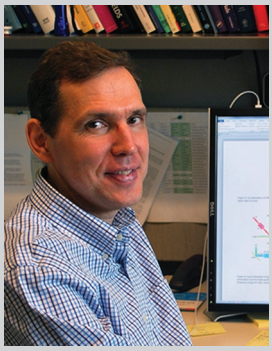

Alexander Kildishev is an associate professor at the Birck Nanotechnology Center, School of Electrical and Computer Engineering, Purdue University. He leads the development of simulation strategies, methods, and software tools for applied electromagnetics and multiphysics simulations of nanoplasmonic systems and optical metadevices. Recent research interests are in the advanced modeling of nanophotonics devices, enhanced light–matter interaction, and transformation optics.